Tuning Negative Thermal Expansion in AlPO 4 -17 by Insertion of Guest Molecules

Frederico Alabarse, Benoît Baptiste, Boby Joseph, Julien Haines

Tuning Negative Thermal Expansion in $AlPO_4$-17 by Insertion of Guest Molecules

Frederico Alabarse[‖], *Benoît Baptiste* [▲], *Boby Joseph* [‖], *and Julien Haines**†

[‖]Elettra Sincrotrone Trieste, Trieste 34149, Italy

[▲] Institut de Minéralogie, de Physique des Matériaux et de Cosmochimie, (IMPMC), UMR 7590 CNRS – Sorbonne Université – IRD – MNHN, 4 place Jussieu, 75252 Paris Cedex 5, France.

† Institut Charles Gerhardt Montpellier, CNRS, Université de Montpellier, ENSCM, 34293 Montpellier, France.

AUTHOR INFORMATION

Corresponding Author

*Julien Haines

Tel: +33448792114

Julien.Haines@umontpellier.fr

ABSTRACT. The very strong negative thermal expansion in the porous aluminophosphate $AlPO_4$-17 with a hexagonal erionite structure was tuned by the insertion of oxygen molecules at high pressure. The structure of the oxygen-filled material was determined in situ at high-pressure by synchrotron, single-crystal x-ray diffraction. The thermal expansion of this material was measured precisely at 0.38 GPa by synchrotron x-ray powder diffraction. Whereas the overall volume thermal expansion only exhibits a small change with respect to empty $AlPO_4$-17 at ambient pressure, the expansion along the *a* direction decreases almost to zero and the expansion along c increases by a factor of 7. Such highly anisotropic thermal expansion properties are of great interest for mechanical and optical applications as in two directions the dimensions of the material are extremely stable, whereas a very strong linear negative thermal expansion of -$2.2x10^{-5}K^{-1}$ is observed in the perpendicular direction. Guest insertion is thus a very powerful tool for tuning the thermal expansion properties of porous materials.

TOC GRAPHICS

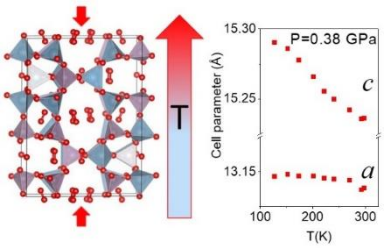

KEYWORDS. Aluminum phosphate, guest insertion, x-ray diffraction, negative thermal expansion, high pressure.

Negative thermal expansion (NTE)[1-10] is a phenomenon that has attracted great interest due to potential mechanical and optical applications. The principal goal is to design materials with low or zero thermal expansion (ZTE) based on compensation by combining a material with positive and another with negative thermal expansion to form a composite. Another strategy for the same types of application is to use directly a material with close to zero volume or linear thermal expansion[11-14]. Typical materials that exhibit NTE and ZTE are those with open framework structures such as oxides, silicates, zeolites, cyanides and metal-organic frameworks, and also perovskites, antiperovskites, glass-ceramics and metal alloys.

In the zeolite family of materials, $AlPO_4$-17, with the hexagonal erionite structure, exhibits the highest coefficient of negative thermal expansion[15-16], $\alpha_V = -3.50 \times 10^{-5}\ K^{-1}$, which is 33% higher than that of the well know NTE framework material ZrW_2O_8[17-18]. The NTE in $AlPO_4$-17 arises from thermally activated transverse oxygen displacements in the Al-O-P units bridging the AlO_4 and PO_4 tetrahedra, which reduce the Al-O-P angles and consequently the Al-P distances in the structure. The framework thus contracts around the empty pores and cages of the structure with increasing temperature. This structure is characterized by 4-, 6-, 8- and 12-membered rings of tetrahedra forming large erionite cages, with a diameter of 6.556 Å, smaller cancrinite cages and double six-membered rings. Atoms or molecules with a maximum kinetic diameter of about 3.4 Å can diffuse into the porosity of this structure via the 8-membered rings. The introduction of small atoms or molecules into the empty cages of $AlPO_4$-17 offers a method to modify its thermal expansion properties by changing the energetics of the transverse motion of the oxygen atoms in the Al-O-P linkages. In the present study, oxygen, with a kinetic diameter[19] of 3.46 Å, was selected to be inserted in $AlPO_4$-17 under high pressure in order to determine the effect of guest insertion on the thermal expansion properties of this material.

In order to measure the thermal expansion of oxygen-filled $AlPO_4$-17 with high precision, a powder sample was studied by x-ray powder diffraction and the data analyzed by full profile refinement, Figure 1. The dehydrated $AlPO_4$-17 powder was loaded with oxygen cryogenically and compressed to 0.39 GPa. Due to insertion of oxygen, the *a* cell parameter increases slightly and *c* decreases strongly with respect to empty $AlPO_4$-17 at ambient pressure and temperature[16] (a=13.08943 Å, c=15.32994 Å). This contrasts with the initial, strong, close to isotropic, compression of empty $AlPO_4$-17 corresponding to the collapse of the empty pores[20]. Variable-temperature, measurements were performed (Figures 1 and 2 and Table 1) on cooling down to a minimum temperature of 127.5 K to avoid solidification of oxygen, while keeping the pressure at 0.38±0.02 GPa.

Table 1. Hexagonal unit cell parameters of $AlPO_4$-17 powder at 0.38±0.01 GPa as a function of temperature.

T(K)	*a*(Å)	*c*(Å)	*V*(Å^3)
298.0	13.1383(8)	15.2361(8)	2277.7(2)
293.0	13.1371(8)	15.2358(7)	2277.2(2)
270.0	13.1440(8)	15.242(7)	2280.4(2)
241.0	13.1446(7)	15.2497(7)	2281.8(2)
222.0	13.1454(7)	15.2554(7)	2283.0(2)
201.0	13.1470(7)	15.2658(7)	2285.1(2)
173.5	13.1468(7)	15.2777(7)	2286.8(2)
152.5	13.1480(7)	15.2857(7)	2288.4(2)
127.5	13.1466(7)	15.2904(7)	2288.6(2)

Expansion along the **a** direction is very close to zero over the temperature range investigated; and particularly over the 127.5-270 K range, whereas there is very strong negative thermal expansion along **c**. The observed value is almost three times higher than the linear thermal expansion in the prototypical NTE material ZrW_2O_8[17-18] and is higher than that of the cyanide $Zn(CN)_2$[21]. As compared to empty $AlPO_4$-17 at ambient pressure, the overall strong negative thermal expansion is retained; however it principally occurs along **c** instead of in the *xy* plane. This indicates that the insertion of guest molecules completely changes the principal direction in which negative thermal expansion occurs. This anisotropic behavior is different with respect to previous reports of the modification of NTE due to guest insertion in materials, such as Prussian Blue analogues, MPt$(CN)_6$, M=Zn,Cd, and YFe$(CN)_6$, in which NTE can be reduced or completely suppressed by the presence of ions or molecules in the pores[22-23], and Li-intercalated ScF_3, in which NTE gradually passes to PTE with Li content[24]. In YFe$(CN)_6$, weak NTE was retained in one direction for certain quantities of K^+ ions and H_2O molecules, but the volume thermal expansion was positive[23]. In the present case in an anisotropic hexagonal material, NTE is only strongly reduced in the *xy* plane and exhibits a strong increase along *z*.

Table 2. Linear and volume thermal expansion coefficients ($10^{-5}K^{-1}$) for oxygen-filled $AlPO_4$-17 at 0.38±0.02 GPa and empty $AlPO_4$-17 at ambient pressure[16].

	O_2-filled $AlPO_4$-17, 0.38(2) GPa	Ambient P[16]
α_a	-0.41(10)	-1.54
α_c	-2.24(10)	-0.45
α_V	-3.07(17)	-3.50

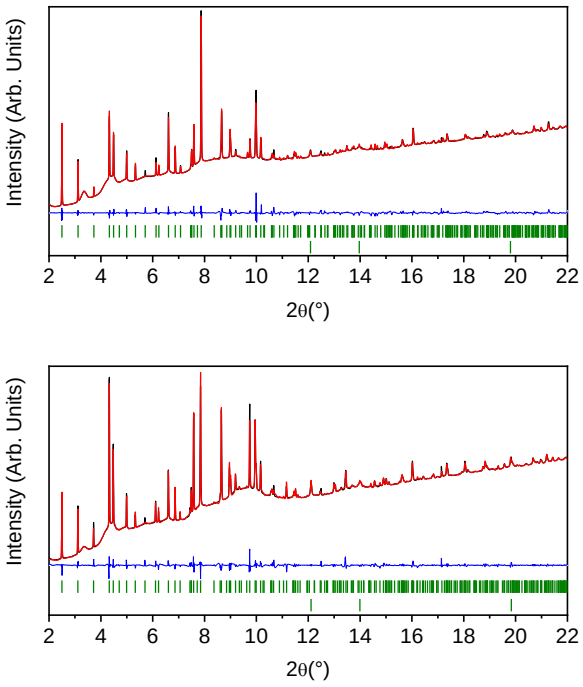

Figure 1. Experimental (black), calculated (red) and difference (blue) profiles (λ=0.4958 Å) for oxygen-filled $AlPO_4$-17 powder at 0.38±0.02 GPa and 293 K (above) and 127.5 K (below). Higher and lower vertical bars indicate the calculated positions of the Bragg reflections of

$AlPO_4$-17 and Au, respectively. The broad signal near 9.6° is due to fluid O_2 and the other broad features are due to the Kapton windows of the cryostat.

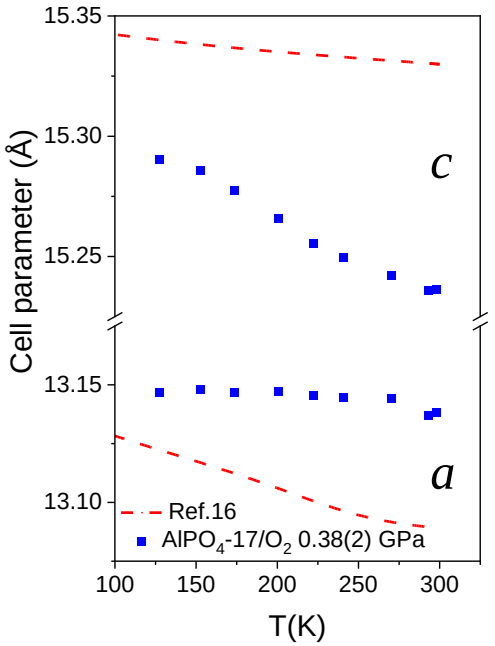

Figure 2. Unit cell parameters (symbols) of oxygen-filled $AlPO_4$-17 powder at 0.38±0.01 GPa as a function of temperature. Data (dashed line) for empty $AlPO_4$-17 at ambient pressure are from Ref. 16.

In order to determine the origin of this close to zero TE in the *xy* plane and the strong NTE along **c**, structure refinements were performed on oxygen-filled AlPO4-17, Table 3 (see also the Crystallographic Information File (CIF file) provided in Supporting Information). A single crystal was investigated at 0.5 GPa in a diamond anvil cell outside the cryostat. Starting from the empty pore structure reported in the literature, Fourier difference maps were used to locate the oxygen

atoms. Nine O_2 molecules were located in the large erionite cages of the structure and a residue corresponding to 0.5 O_2 molecules in the small cancrinite cages, Figure 3. No electron density was located in the double six-membered rings that link the cancrinite cages to form pillars along **c**. This gives a total of 19 O_2 molecules per unit cell and an overall chemical formula of $AlPO_4 \cdot 1.06O_2$. The introduction of O_2 has a major impact on the unit cell and the structure when comparing empty $AlPO_4$-17 (a=13.08943 Å, c=15.32994 Å)[16] at ambient pressure and the O_2-filled material at 0.5 GPa (a=13.1181(6) Å, c=15.246(1) Å). The unit cell volumes are very similar. The insertion of oxygen results in an expansion in the *xy* plane and an increase in the diameter of the erionite cages from 6.556 Å at ambient pressure[16] to 6.633(1) Å. The effect of oxygen insertion is very different from the effect of pressure, which initially compresses the structure close to isotropically (*a*=13.0463 Å, *c*=15.2907 Å at 0.43 GPa) in non-penetrating silicone oil, before the onset of elastic softening[20]. Such isotropic elastic behavior would not be expected to induce a major relative change in the NTE behavior along *a* and *c* in empty-pore $AlPO_4$-17. In isotropic, cubic $Zn(CN)_2$, an enhancement of NTE behavior is observed at high pressure[25]. The mechanism of negative thermal expansion is considered to be due to thermally excited, transverse motion of oxygen atoms in the Al-O-P units bridging the tetrahedra[16]. Such motion in the xy plane can be expected to be reduced due to the strain induced in the expanded cages in this plane due to the presence of the O_2 molecules, which cause damping of these vibrations. Thermal ellipsoids provide direct information on tranverse atomic displacement in NTE materials[22-29]. It can be noted that the components of the thermal ellipsoids of many framework oxygen atoms in $AlPO_4$-17 are greater along the *c* direction than in the *xy* plane indicating greater transverse thermal vibration in this direction (Figure 4 and Table S1in Supporting Information) and greater rigidity in the *xy* plane. Negative thermal expansion is thus favored along the *c* direction, where *c* tends at low temperature towards the

corresponding value of the empty structure at room pressure upon reduction of the transverse motion of oxygen. It can be noted that under pressure the *c* direction exhibits compression rather than expansion in spite of the insertion of oxygen molecules, which is consistent with flexibility being retained along this direction. This compression is greater than that observed for the empty material between room pressure and 0.43 GPa.

The concept of average atomic volume (AAV)[30] has been recently established to predict isotropic NTE behavior, based on the principle that the more open and flexible the structure is the stronger the NTE effect is observed. A critical AAV of close to 16 $Å^3$ exists below which the coefficient of thermal expansion (CTE) passes from negative to positive. Empty $AlPO_4$-17 has an AAV of 21.1 $Å^3$ consistent with strong NTE. Upon filling with O_2 molecules, the AAV decreases to 15.6 $Å^3$ just below the critical value; however, the CTE decreases by only about 15%. In this anisotropic material, the ZTE expected at the critical value is approached only in the *xy* plane. The reduction in flexibility appears to be distinct in anisotropic materials. It can also be noted that the O_2 molecules interacting by van der Waals forces have much greater degrees of freedom to reorient and translate than framework atoms linked by covalent bonds, thus some flexibility can be retained.

Table 3. Atomic coordinates and equivalent isotropic displacement parameters for O_2–filled $AlPO_4$-17 at 0.5 GPa. U_{eq} is defined as one third of the trace of the orthogonalized U_{ij} tensor.

	x	y	z	U_{eq} ($Å^2$)
P(1)	0.9978(2)	0.2358(2)	0.1019(1)	0.032(1)
P(2)	0.5742(2)	0.9070(2)	0.25	0.029(1)

Al(2)	0.0931(3)	0.4245(2)	0.25	0.028(1)
Al(1)	0.7628(2)	0.9981(2)	0.1014(1)	0.029(1)
O(1)	0.0254(4)	0.3423(4)	0.1581(3)	0.040(1)
O(1')	0.6470(4)	0.9667(5)	0.1679(3)	0.044(1)
O(2)	0.906(5)	0.1990(5)	0.160(4)	0.050(2)
O(3)	0.1331(4)	0.2550(4)	0.6280(3)	0.040(1)
O(4)	0.2730(5)	0.0031(5)	0.0060(3)	0.050(2)
O(5)	0.2376(6)	0.4600(6)	0.25	0.044(2)
O(6)	0.4643(5)	0.9194(6)	0.25	0.034(2)
O(11)	0.2569(19)	0.5100(20)	0.7810(20)	0.338(16)
O(12)	0.4271(19)	-0.1420(20)	0.9678(19)	0.274(12)
O(13)	0.4160(20)	-0.1740(30)	0.0270(20)	0.306(14)
O(14)	0	0	0.25	0.440(50)

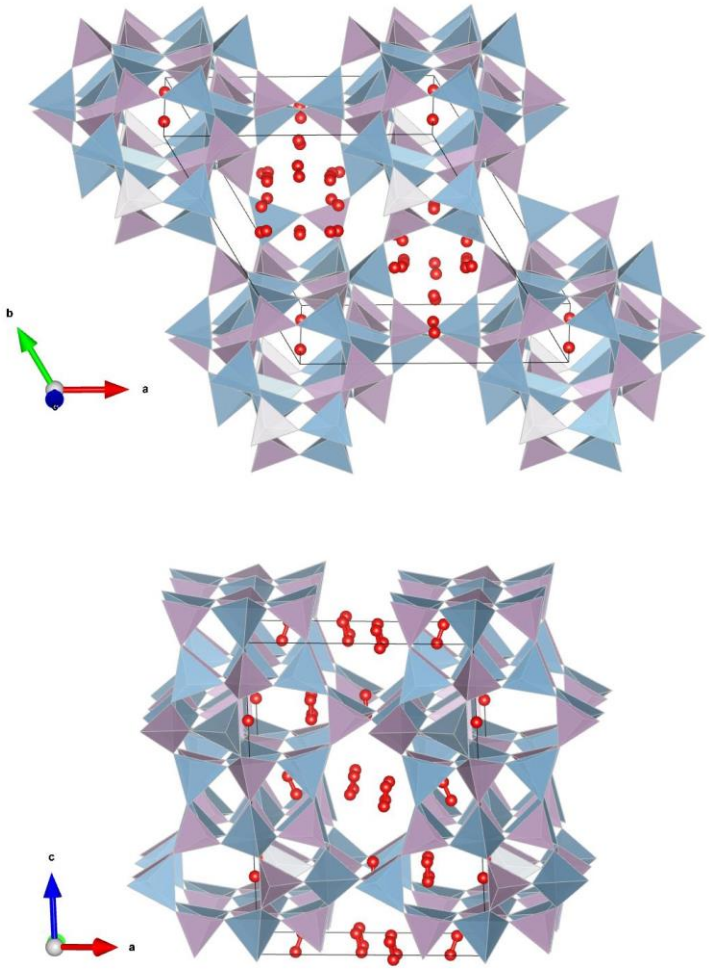

Figure 3. Views of the crystal structure of O_2–filled $AlPO_4$-17 at 0.5 GPa.

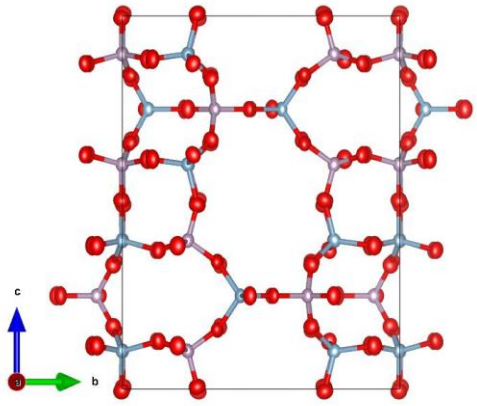

Figure 4. The crystal structure of O_2–filled $AlPO_4$-17 at 0.5 GPa with thermal ellipsoids (the O_2 molecules are not shown for clarity).

This material is particularly interesting as it exhibits close to zero thermal expansion in the *xy* plane over an extended temperature range from 270 K down to at least 127.5 K due to filling of the pores of $AlPO_4$-17 by guest molecules. This indicates that the thermal expansion properties of a porous host can be tuned by guest insertion thus opening a way to design zero thermal expansion materials. Selection of non-volatile guests or the polymerization of the guest molecules[31-35] would provide new materials for mechanical and optical applications.

Experimental Methods

Single crystals of hydrated $AlPO_4$-17 with maximum dimensions of 250 × 70 × 70 μm^3 were synthesized as described previously[20, 36] from aluminum triisopropoxide and phosphoric acid using N,N,N′,N′-tetramethyl-1,6-hexanediamine as a structure directing agent. The crystals were calcined in air at 500°C for 24 h.

For the high-pressure x-ray powder diffraction experiments, $AlPO_4$-17 single crystals were ground and placed in a 220 μm diameter and 86 μm thick stainless steel gasket along with the pressure and temperature calibrants (ruby, samarium-doped strontium borate, gold) in a membrane diamond anvil cell. The DAC was placed in the cryogenic gas loading system and the sample was dehydrated for 2h at 110°C under vacuum (4 Pa). Oxygen was then loaded cryogenically by condensing oxygen gas. The DAC was then placed in an AlmaxEasylab (JANIS) He cryostat and measurements were performed on cooling.

Ruby and samarium-doped strontium borate were used as pressure calibrants and gold as a temperature calibrant, respectively. The temperature was measured with a thermocouple placed on the diamond anvil. The thermocouple temperature was always within 1 K from that calculated from the thermal expansion of the Au calibrant[37]. The pressure was measured and controlled to a value of 0.38±0.02 GPa based on the shift in the $^7D_0$–$^5F_0$ fluorescence line of samarium-doped strontium borate[38-39] and in the R_1 fluorescence line of ruby corrected for the sample temperature[40-41].

In the case of the single crystal study, a crystal with dimensions of 190 × 70 × 70 μm^3, was placed in a 250 μm diameter and 95 μm thick stainless steel gasket in a membrane DAC. Dehydration and cryogenic loading were performed as in the powder experiment.

X-ray diffraction measurements (λ=0.4958 Å) under pressure were performed with an 80 μm beam on the Xpress beamline equipped with a PILATUS3 S 6M (DECTRIS) detector placed at 950.69 mm from the sample at the Elettra Sincrotrone Trieste (Trieste, Italy). The XRD images were converted to 1-D diffraction profiles using Dioptas[42]. Le Bail and Rietveld refinements were performed using Fullprof[43]. Le Bail and Rietveld refinements gave identical cell parameters;

however, there are too many free atomic fractional coordinates to get accurate interatomic distances and angles for $AlPO_4$-17.

The $AlPO_4$-17 single crystal was studied on the same beam line with the detector placed at 279.00 mm from the single crystal sample. Diffraction data were collected using a phi scan from –30° to +30°. Data reduction was performed with CrysalisPro 1.171.39.46 (Rigaku OD, 2018). The crystal structure was refined using Shelxl-2017/1[44] with the WinGX[45] interface. Crystal structures plotted using Vesta[46].

ASSOCIATED CONTENT

Supporting Information.

The following file containing the Crystallographic Information File for $AlPO_4$-17 /O_2 at 0.5 GPa and the table S1 with the principal axes of the anisotropic thermal ellipsoids of the framework oxygen atoms is available free of charge.

Alabarse_jz-2022-0271Bu_SI.pdf (PDF)

AUTHOR INFORMATION

Notes

The manuscript was written through contributions of all authors. All authors have given approval to the final version of the manuscript. The authors declare no competing financial interests.

ACKNOWLEDGMENTS

The research leading to this result has been supported by the project CALIPSOplus under Grant Agreement 730872 from the EU Framework Programme for Research and Innovation HORIZON 2020. The synchrotron X-ray diffraction experiments were performed at the Xpress

beamline from Elettra Sincrotrone Trieste (proposal numbers: 20200249, 20215637). We acknowledge R. Borghes and V. Chenda for having improved the Xpress beamline software tools and for I. Cudin and M. Barnaba for their improvements on the cryostat configuration.

REFERENCES

1. Evans, J. S. O. Negative thermal expansion materials. *J. Chem. Soc. Dalton.* **1999,** , 3317-3326.
2. Barrera, G. D.; Bruno, J. A. O.; Barron, T. H. K.; Allan, N. L. Negative thermal expansion. *J. Phys.-Condens. Mat.* **2005,** *17*, R217-R252.
3. Miller, W.; Smith, C. W.; Mackenzie, D. S.; Evans, K. E. Negative thermal expansion: a review. *J. Mater. Sci.* **2009,** *44*, 5441-5451.
4. Lind, C. Two decades of negative thermal expansion research: where do we stand? *Materials* **2012,** *5*, 1125-1154.
5. Takenaka, K. Negative thermal expansion materials: technological key for control of thermal expansion. *Sci. Technol. Adv. Mater.* **2012,** *13*, 013001.
6. Takenaka, K. Progress of research in negative thermal expansion materials: paradigm shift in the control of thermal expansion. *Front. Chem.* **2018,** *6*, 267.
7. Attfield, J. P. Mechanisms and materials for NTE. *Front. Chem.* **2018,** *6*, 371.
8. Coates, C. S.; Goodwin, A. L. How to quantify isotropic negative thermal expansion: magnitude, range, or both? *Mater. Horizons* **2019,** *6*, 211-218.
9.Liang, E. J.; Sun, Q.; Yuan, H. L.; Wang, J. Q.; Zeng, G. J.; Gao, Q. L. Negative thermal expansion: Mechanisms and materials. *Front. Phys.* **2021,** *16*, 53302.
10. Shi, N.; Song, Y.; Xing, X.; Chen, J. Negative thermal expansion in framework structure materials. *Coordin Chem Rev* **2021,** *449,* 214204.
11. Salvador, J. R.; Gu, F.; Hogan, T.; Kanatzidis, M. G. Zero thermal expansion in YbGaGe due to an electronic valence transition. *Nature* **2003,** *425* (6959), 702-705.
12. Margadonna, S.; Prassides, K.; Fitch, A. N. Zero thermal expansion in a Prussian blue analogue. *J Am Chem Soc* **2004,** *126* (47), 15390-15391.
13. Marinkovic, B. A.; Ponton, P. I.; Romao, C. P.; Moreira, T.; White, M. A. Negative and Near-Zero Thermal Expansion in $A_2M_3O_{12}$ and Related Ceramic Families: A Review. *Front. Mater.* **2021,** *8*, 741560
14. Liu, J. N.; Maynard-Casely, H. E.; Brand, H. E. A.; Sharma, N. $Sc_{1.5}Al_{0.5}W_3O_{12}$ exhibits zero thermal expansion between 4 and 1400 K. *Chem Mater* **2021,** *33* (10), 3823-3831.
15. Tschaufeser, P.; Parker, S. C. Thermal-expansion behavior of zeolites and $AlPO_4$s. *J Phys Chem-Us* **1995,** *99* (26), 10609-10615.
16. Attfield, M. P.; Sleight, A. W. Exceptional negative thermal expansion in $AlPO_4$-17. *Chem. Mater.* **1998,** *10* (7), 2013-2019.
17. Mary, T. A.; Evans, J. S. O.; Vogt, T.; Sleight, A. W. Negative thermal expansion from 0.3 to 1050 Kelvin in ZrW_2O_8. *Science* **1996,** *272* (5258), 90-92.
18. Evans, J. S. O.; Mary, T. A.; Vogt, T.; Subramanian, M. A.; Sleight, A. W. Negative thermal expansion in ZrW_2O_8 and HfW_2O_8. *Chem. Mater.* **1996,** *8* (12), 2809-2823.

19. Breck, D. W. *Zeolite Molecular Sieves: Structure, Chemistry and Use.* John Wiley & Sons, Inc: New York, 1974.
20. Alabarse, F. G.; Silly, G.; Brubach, J. B.; Roy, P.; Haidoux, A.; Levelut, C.; Bantignies, J. L.; Kohara, S.; Le Floch, S.; Cambon, O.; Haines, J. Anomalous compressibility and amorphization in $AlPO_4$-17, the oxide with the highest negative thermal expansion. *J. Phys. Chem. C* **2017,** *121* (12), 6852-6863.
21. Chapman, K. W.; Chupas, P. J.; Kepert, C. J. Direct observation of a transverse vibrational mechanism for negative thermal expansion in $Zn(CN)_2$: An atomic pair distribution function analysis. *J. Am. Chem. Soc.* **2005,** *127* (44), 15630-15636.
22. Goodwin, A. L.; Chapman, K. W.; Kepert, C. J. Guest-dependent negative thermal expansion in nanoporous Prussian Blue analogues $M^{II}Pt^{IV}(CN)_6{\cdot}x\{H_2O\}$ ($0 \leq x \leq 2$; M = Zn, Cd). *J. Am. Chem. Soc.* **2005,** *127*, 17980-17981.
23. Gao, Q. L.; Chen, J.; Sun, Q.; Chang, D. H.; Huang, Q. Z.; Wu, H.; Sanson, A.; Milazzo, R.; Zhu, H.; Li, Q.; Liu, Z. N.; Deng, J. X.; Xing, X. R. Switching between giant positive and negative thermal expansions of a $YFe(CN)_6$-based Prussian Blue analogue induced by guest species. *Angew. Chem. Int. Edit.* **2017,** *56*, 9023-9028.
24. Chen, J.; Gao, Q. L.; Sanson, A.; Jiang, X. X.; Huang, Q. Z.; Carnera, A.; Rodriguez, C. G.; Olivi, L.; Wang, L.; Hu, L.; Lin, K.; Ren, Y.; Lin, Z. S.; Wang, C.; Gu, L.; Deng, J. X.; Attfield, J. P.; Xing, X. R. Tunable thermal expansion in framework materials through redox intercalation. *Nat. Commun.* **2017,** *8*, 14441.
25. Chapman, K. W.; Chupas, P. J. Pressure enhancement of negative thermal expansion behavior and induced framework softening in zinc cyanide. *J. Am. Chem. Soc.* **2007,** *129*, 10090-10091.
26. Shi, N.; Sanson, A.; Gao, Q. L.; Sun, Q.; Ren, Y.; Huang, Q. Z.; de Souza, D. O.; Xing, X. R.; Chen, J. Strong Negative Thermal Expansion in a Low-Cost and Facile Oxide of $Cu_2P_2O_7$. *J. Am. Chem. Soc.* **2020,** *142*, 3088-3093.
27. Gao, Q. L.; Sun, Y.; Shi, N. K.; Milazzo, R.; Pollastri, S.; Olivi, L.; Huang, Q. Z.; Liu, H.; Sanson, A.; Sun, Q.; Liang, E. J.; Xing, X. R.; Chen, J. Large isotropic negative thermal expansion in water-free Prussian blue analogues of $ScCo(CN)_6$. *Scripta Mater.* **2020,** *187*, 119-124.
28. Goodwin, A. L.; Kepert, C. J. Negative thermal expansion and low-frequency modes in cyanide-bridged framework materials. *Phys. Rev. B* **2005,** *71*, 140301.
29. Wei, Z. S.; Tan, L.; Cai, G. Q.; Phillips, A. E.; da Silva, I.; Kibble, M. G.; Dove, M. T. Colossal Pressure-Induced Softening in Scandium Fluoride. *Phys. Rev. Lett.* **2020,** *124*, 255502.
30. Gao, Q. L.; Wang, J. Q.; Sanson, A.; Sun, Q.; Liang, E. J.; Xing, X. R.; Chen, J. Discovering Large Isotropic Negative Thermal Expansion in Framework Compound $AgB(CN)_4$ via the Concept of Average Atomic Volume. *J. Am. Chem. Soc.* **2020,** *142*, 6935-6939.
31. Santoro, M.; Gorelli, F. A.; Bini, R.; Haines, J.; van der Lee, A. High-pressure synthesis of a polyethylene/zeolite nano-composite material. *Nat. Commun.* **2013,** *4,* 1557.
32. Scelta, D.; Ceppatelli, M.; Santoro, M.; Bini, R.; Gorelli, F. A.; Perucchi, A.; Mezouar, M.; van der Lee, A.; Haines, J. High pressure polymerization in a confined space: conjugated chain/zeolite nanocomposites. *Chem. Mater.* **2014,** *26*, 2249-2255.
33. Santoro, M.; Dziubek, K.; Scelta, D.; Ceppatelli, M.; Gorelli, F. A.; Bini, R.; Thibaud, J. M.; Di Renzo, F.; Cambon, O.; Rouquette, J.; Hermet, P.; van der Lee, A.; Haines, J. High pressure synthesis of all-transoid polycarbonyl $[-(C{=}O)-]_n$ in a zeolite. *Chem. Mater.* **2015,** *27*, 6486-6489.

34. Santoro, M.; Scelta, D.; Dziubek, K.; Ceppatelli, M.; Gorelli, F. A.; Bini, R.; Garbarino, G.; Thibaud, J. M.; Di Renzo, F.; Cambon, O.; Hermet, P.; Rouquette, J.; van der Lee, A.; Haines, J. Synthesis of 1D polymer/zeolite nanocomposites under high pressure. *Chem. Mater.* **2016,** *28*, 4065-4071.
35. Alabarse, F. G.; Polisi, M.; Fabbiani, M.; Quartieri, S.; Arletti, R.; Joseph, B.; Capitani, F.; Contreras, S.; Konczewicz, L.; Rouquette, J.; Alonso, B.; Di Renzo, F.; Zambotti, G.; Bau, M.; Ferrari, M.; Ferrari, V.; Ponzoni, A.; Santoro, M.; Haines, J. High-pressure synthesis and gas-sensing tests of 1-D polymer/aluminophosphate nanocomposites. *ACS Appl. Mater. Inter.* **2021,** *13*, 27237-27244.
36. Tuel, A.; Lorentz, C.; Gramlich, V.; Baerlocher, C. AIPO-ERI, an aluminophosphate with the ERI framework topology: characterization and structure of the as-made and calcined rehydrated forms. *CR Chim.* **2005,** *8*, 531-540.
37. Anderson, O. L.; Isaak, D. G.; Yamamoto, S. Anharmonicity and the equation of state for gold. *J. Appl. Phys.* **1989,** *65*, 1534-1543.
38. Lacam, A.; Chateau, C. High-pressure measurements at moderate temperatures in a diamond anvil cell with a new optical sensor - SrB_4O_7-Sm^{2+}. *J. Appl. Phys.* **1989,** *66*, 366-372.
39. Datchi, F.; LeToullec, R.; Loubeyre, P. Improved calibration of the SrB_4O_7:Sm^{2+} optical pressure gauge: Advantages at very high pressures and high temperatures. *J. Appl. Phys.* **1997,** *81*, 3333-3339.
40. Datchi, F.; Dewaele, A.; Loubeyre, P.; Letoullec, R.; Le Godec, Y.; Canny, B. Optical pressure sensors for high-pressure-high-temperature studies in a diamond anvil cell. *High Pressure Res* **2007,** *27*, 447-463.
41. Shen, G.; Wang, Y.; Dewaele, A.; Wu, C.; Fratanduono, D. E.; Eggert, J.; Klotz, S.; Dziubek, K. F.; Loubeyre, P.; Fat'yanov, O. V.; Asimow, P. D.; Mashimo, T.; Wentzcovitch, R. M. M.; Bass, J.; Bi, Y.; He, D.; Khishchenko, K. V.; Leinenweber, K.; Li, B.; Sakai, T.; Tsuchiya, T.; Shimizu, K.; Yamazaki, D.; Mezouar, M.; Grp, I. T. Toward an international practical pressure scale: A proposal for an IPPS ruby gauge (IPPS-Ruby2020). *High Pressure Res.* **2020,** *40*, 299-314.
42. Prescher, C.; Prakapenka, V. B. DIOPTAS: a program for reduction of two-dimensional X-ray diffraction data and data exploration. *High Pressure Res.* **2015,** *35*, 223-230.
43. Rodriguez-Carvajal, J. Magnetic structure determination from powder diffraction using the program FullProf. *Applied Crystallography* **2001**, 30-36.
44. Sheldrick, G. M. Crystal structure refinement with SHELXL. *Acta Crystallogr. Section C-Structural Chemistry* **2015,** *71*, 3-8.
45. Farrugia, L. J. WinGX and ORTEP for Windows: an update. *J. Appl. Crystallogr.* **2012,** *45*, 849-854.
46. Momma, K.; Izumi, F. VESTA 3 for three-dimensional visualization of crystal, volumetric and morphology data. *J. Appl. Crystallogr.* **2011,** *44*, 1272-1276.